RSC Pharmaceutics

ROYAL SOCIETY OF CHEMISTRY

PAPER

View Article Online
View Journal

Cite this: DOI: 10.1039/d5pm00259a

Polymersomal delivery enhances third-generation photodynamic therapy with the first white-light-activated peptide photosensitiser for melanoma

Talat Nahid Khan,[a,b] Mohammed Naeem Khan,[a,b] Poullette R. Oduor,[b] Heather Nesbitt,[a] Thomas McKaig,[a] Anthony P. McHale,[a] John F. Callan[a] and Bridgeen Callan *[a,b]

Photodynamic therapy (PDT) is an established cancer treatment, yet its clinical utility in melanoma remains restricted by poor photosensitiser delivery, light penetration, and melanin interference. Here, we report a polymersomal nanocarrier system encapsulating the peptide–photosensitiser conjugate RB-K2 as a novel strategy to overcome these barriers. The polymersomes, engineered from amphiphilic block copolymers, demonstrated enhanced stability and efficient tumour-targeted delivery. *In vitro*, PS-RB-K2 significantly improved cellular uptake, reactive oxygen species generation, and apoptosis induction in B16 melanoma cells compared with free RB-K2. *In vivo*, intratumoural administration of PS-RB-K2, combined with optimised light activation, markedly suppressed tumour growth and, in some cases, reversed progression without systemic toxicity. Mechanistic analyses confirmed that polymersomal encapsulation protected RB-K2 from degradation, enhanced intratumoural retention, and mitigated self-quenching effects. Collectively, these findings establish PS-RB-K2 as a potent third-generation PDT platform with translational potential for melanoma therapy, bridging the gap between current liposomal systems and clinically viable polymersomal drug delivery.

Received 22nd September 2025,
Accepted 2nd December 2025

DOI: 10.1039/d5pm00259a

rsc.li/RSCPharma

1.0. Introduction

1.1. Polymersomes in cancer therapy

Polymersomes, vesicular nanocarriers formed from self-assembling amphiphilic block copolymers, have emerged as promising platforms for cancer therapy. Owing to their superior structural stability, tunability, and ability to encapsulate both hydrophilic and hydrophobic agents, they offer advantages over traditional delivery systems like micelles and liposomes.[1] Moreover, their versatility allows for the integration of targeting ligands, stimuli-responsive components, and imaging agents—making them ideal candidates for use in advanced generations of therapeutic drug delivery.

Liposomes are the prototypical self-assembly structures for a variety of nanoparticles, including polymersomes and have been investigated and employed as nanovesicles for drug administration and as a model simulating cell membrane since the 1970s.[2] Polymersomes on the other hand were first acknowledged in the 1990s and since then have become an attractive alternative to liposomes owing to their enhanced stability *via* altering vesicles membrane characteristics such as strength and durability, permeability, and surface adaptivity.[3] There are number of polymers approved by the FDA for fabricating a variety of formulations such as PLA-*b*-PEG-*b*-PLA (polylactic acid-*b*-polyethylene glycol-*b*-polylactic acid tri-block polymer), and PLH-*b*-PEG (poly(L-histidine)-*b*-polyethylene glycol polymer).[4] Genexol®PM is an example of a commercially available polymeric micelle containing paclitaxel created from mPEG-PDLLA (monomethoxy-poly(ethylene glycol)-*block*-poly (D,L-lactide)) polymer and used for the treatment of breast cancer.[5]

Despite extensive preclinical research, there is limited evidence of polymersome-based systems having reached human clinical trials.[6–8] However, non-vesicular polymeric nanocarriers like CRLX101[9,10] have undergone phase I–II trials, validating the core polymer chemistry and biocompatibility with ACM Biolabs (2025) progressing a polymer/lipid hybrid as a non-viral delivery system capable of delivering multiple payloads, suggesting that translation to the clinic is on the horizon.

1.2. Photodynamic therapy and polymersomes

Photodynamic therapy (PDT) is a minimally invasive cancer treatment that combines a photosensitizing agent, light, and

[a]*Biomedical Sciences Research Institute, University of Ulster, Coleraine, Northern Ireland, BT52 1SA, UK. E-mail: b.callan@ulster.ac.uk*
[b]*Klas Therapeutics Limited, c/o 50 Bedford Street, Belfast, Northern Ireland, BT27FW, UK*

oxygen to selectively kill cancer cells. It causes localized cell death through the production of reactive oxygen species (ROS), particularly singlet oxygen ($^1O_2$), when the photosensitizer is activated by a specific wavelength of light. It is currently approved for use in oesophageal cancer, non-small cell lung cancer (NSCLC), bladder cancer, head and neck tumours and basal cell carcinoma with current trials underway for glioblastoma,[11] pancreatic cancer[12] and cholangiocarcinoma.

Foslip® and Fospeg® are liposomal preparations of the marketed formulation Foscan®, which contains the photosensitising compound, temoporfin as an active ingredient and has been medically used to treat advanced stages of head and neck cancer in patients who have failed to respond to other treatments or are not candidates for other forms of therapy or surgery.[13,14] There are currently no commercially available polymersomal alternative to these liposomal formulations, however, a few examples are under preclinical development. Several researchers have studied various polymeric delivery systems for encapsulation of photosensitising agents for PDT treatment for enhanced delivery and efficacy.[15–17] Furthermore, a number of researchers are exploiting the advantageous effects of PDT efficacy seen from the encapsulation of the photosensitiser compound and enhancing this by combining with a second different therapy.[17–19]

1.3. Polymersomes with PDT in melanoma

The use of PDT for melanoma is limited, due in part to the highly pigmentated nature of the melanin present in melanoma cells. Only a few examples can be found within literature where novel pathways have been exploited to expand the use of PDT into melanoma, however, none of them use a white light source for activation of a peptide-photosensitiser conjugate. Lu *et al.* (2020)[20] utilise a β-alanine modified fullerene-based nanoparticles (GFNPs), ~126 nm in diameter, optimized for size-dependent effects. Upon light activation, GFNPs generated singlet oxygen ($^1O_2$) to selectively disrupt tumour blood vessels-even in hypoxic melanoma microenvironments. Although PDT is used as the mechanism of action, the solid fullerene-based nanoparticles have limited capacity for encapsulation of different compounds as this is mostly restricted to surface absorption. Translation to the clinic for these solid particles may be somewhat hampered due to the use of the rare earth metal gadolinium. Tang *et al.* (2020)[21] combined a near infrared activated photosensitiser with chemotherapy, while Wang *et al.* (2017)[22] reported the activation of a photosensitiser encapsulated within a polymersome and activated using cold atmospheric plasma (CAP), both of which may require expensive activation equipment with specialist handling. More recently Tsai *et al.* (2025)[23] report the creation and investigation into PEGylated chitosan-coated polydopamine nanoparticles (PCPNs) that release the anticancer agent IR780 in acidic tumour environments. Under near-infrared (NIR) light, the IR780@PCPNs show strong photothermal and photodynamic effects, generating heat and reactive oxygen species to kill melanoma cells effectively as a combination approach for enhanced efficacy, however this has not been proven *in vivo*. We have previously reported a novel PDT agent for use against melanoma[24] using a unique peptide photosensitiser conjugate, known as RB-K2. The combination of the pro apoptotic peptide conjugated to the photosensitiser, rose bengal, resulted in a 500% reduction in melanoma tumour growth in the murine model, and is currently under continued investigation as a novel first in class treatment for melanoma (Klas Therapeutics Ltd).

The potential of these systems to be designed and utilised for multiple uses is still to reach its full potential. This paper describes the enhanced efficacy of a novel polymersomal based drug delivery system in combination with RB-K2 utilising PDT for the treatment of melanoma, skin cancer. The extensive pre-clinical evidence takes this technology a step closer to the bridging the gap between liposomal DDS and polymersomal DDS in the clinic and opens the door for PDT as a treatment option for melanoma.

2.0. Study aims

This study investigates the enhanced potential of PDT for melanoma using the peptide conjugate RB-K2 encapsulated within a polymersomal drug delivery system, PS-RB-K2. We have already evidenced the superior efficacy of RB-K2 compared with other photosensitisers for the use in melanoma,[24] here, we expand this technology by the inclusion of nanotechnology for enhanced uptake and protection from degradation, creating the third-generation PDT for melanoma.

3.0. Materials and methods

3.1. Materials

DMEM (Dulbecco's Modified Eagle's medium), penicillin streptomycin (PenStrep) and FBS (foetal bovine) serum was purchased from (Thermofisher Scientific, UK), TFA (trifluoroacetic acid reagentplus(r) 99%) (Honeywell), acetonitrile, and chloroform, were analytical grade and were purchased from (Thermofisher Scientific, UK). PEG-methacrylate (M_n 500) (SIGMA-ALDRICH), ABCN (1,1′-azobis(cyclohexanecarbonitrile), 98%) (SIGMA-ALDRICH), THF (tetrahydrofuran, anhydrous, ≥99.9%) (SIGMA-ALDRICH), LED torches were used as a source for white light – Fenix LD01 LED (Fenix Light Ltd, Shenzen, China) 50 mW output, MTT (thiazolyl blue tetrazolium bromide) (Applichem Lifescience), DMSO (dimethyl sulfoxide – ACS grade) (VWR chemicals), Annexin V-iFluor 488 Apoptosis Detection Kit (ab219916) bought from (Abcam). All the cells were obtained from in house cell repository, CD-1 Nude mice were bread inhouse.

3.1. Synthesis and purification of RB-K2

Synthesis of RB-K2 was achieved using solid phase peptide synthesis according to a previously published method.[25] To purify the peptide RB-K2, reversed-phase high performance liquid chromatography (RP-HPLC) was utilised, and the gradi-

ent of solvent-B was raised from 45 to 65 percent over a 25-minute period. The solvents used were – solvent-A, which included combination of 89.9% deionised water, 10% acetonitrile, and 0.1% trifluoroacetic acid (TFA), and solvent-B, contained 99.9% acetonitrile and 0.1% TFA. The required fraction of RB-K2 was collected between 11.0–12.5 minutes and analysed using the wavelength range 560–575 nm. The sample was analysed using MALDI-TOF-MS to indicate the presence of compound with the anticipated mass. The collected fractions were combined, and the solvent removed by rotary evaporation and lyophilisation to obtain the dry peptide sample as a pink solid.

3.2. Synthesis and purification of polymer

The polymer used in the formulation of polymersomes were synthesised by the method described by Martin C. *et al.* (2016).[26] Briefly, the random co-polymer has two moieties: decyl methacrylate and PEG methacrylate (M_n 500) accounting for 37.5% w/w and 62.5% w/w respectively. Polymerisation was achieved *via* a Michael addition reaction using a free radical initiator ABCN (1,1′-azobis(cyclohexanecarbonitrile)) to generate the random copolymer of known configuration. Purification of the polymer was achieved by precipitation of the polymeric solution in THF (tetrahydrofuran) and hexane. The solution was centrifuged to obtain a pellet of the polymer. The supernatant was discarded, and the polymer was dissolved again in a minimal amount of THF and precipitated with hexane, followed by centrifugation yielding the desired polymer. The process of dissolving in THF and precipitating out in hexane was repeated several times until the polymer appeared transparent.

3.3. Preparation of polymersomes

The formulation of PS was carried out using the amphiphilic polymer previously described. Briefly, 0.5 ml of polymer (5 mg ml^{-1} in chloroform) was added to a 5 ml round bottom flask, the solvent was evaporated to dryness producing a thin film along the base of the flask. RB-K2 at a concentration of 400 μM (400 μl 1 mM) in methanol was added to the flask and again evaporated to dryness. The thin film of both polymer and drug was resuspended in organic solvent (0.5 ml chloroform) and sonicated for 15 min at room temperature (Branson 2800, CPX280H-E, 110 W, 40 kHz). A further 0.5 mL polymer (5 mg ml^{-1}) was added in PBS with 30 min sonication to create an opaque emulsion followed by rotary evaporation to remove any trace of the organic solvent (chloroform) leaving the final nanoparticles as a clear PBS suspension.

PS were evaluated for poly dispersibility index (PDI) and hydrodynamic radius using dynamic light scattering (DLS). The measurement of PDI and size were taken at room temperature and in triplicate.

3.4. *In vitro* analysis

3.4.1. MTT cell viability assay. B-16 melanoma cells were cultured in complete DMEM (Dulbecco's Modified Eagle's medium), which was supplemented with 10%(v/v) FBS (Fetal Bovine Serum) and 1%(v/v) penicillin streptomycin mixture. The cells were cultured at 37 °C, in an incubator maintained at a relative humidity-95%, 5%-CO2, 20%-O2, and were harvested for experiment when they reached a confluency of between 70–80%. The cells were seeded into 96 well plates, with 4000 cells in 100 μl of complete media. After incubation for 24 h, the cells were incubated with 100 μl of treatment samples at indicated concentrations for 3 h and kept away from light. Following treatment, the cells were washed twice with 100 μl of PBS and 100 μl of fresh culture media was added to each well. The cells were further treated with white light (Fenix LD01 LED, 50 mW output) for either 0, 1 or 2 minutes (0, 22.8, 45.6 J cm^{-2}). Cells were incubated for 24 h after treatment at the conditions previously stated. After which time the cells were incubated with 10 μl of MTT (tetrazolium salt) solution (5 mg of MTT per 1 ml of PBS) for 3 h followed by the replacement of solution in the wells with 100 μl of DMSO. The absorbance of the resulting formazan solution was measured at 570 nm using a Fluostar Omega microplate reader to determine cell viability. The cell viability was calculated by the formula below.

$$\%\,\text{Cell viability} = \frac{\text{average absorbance of sample}}{\text{average absorbance of untreated sample}} \times 100$$

3.4.2. Cellular uptake study. Cells were cultured, harvested, and seeded in a similar manner as stated above. The cells were incubated with 5 μM either RB-K2 or PS-RB-K2 for 3 h followed by washing with PBS (×2). Later 100 μl of PBS was added in each well. The fluorescence intensity was recorded on BMG labtech Omega microplate reader with an excitation wavelength of 550 nm and emission at 590 nm at 2100 gain and compared to a control well (dark) with no treatment.

3.4.3. Apoptosis assay carried out *in vitro* in B16 cells. Apoptosis assay in B16 cells using 1 μM samples of RB-K2 and PS-RB-K2 was carried out with or without stimulating the samples for 1 min light (Fenix LD01 LED, 50 mW output, 22.8 J cm^{-2}) and compared directly with healthy cells in individual groups. The experiment was carried out in a similar manner as detailed for PDT experiment in section 3.4.1. The obtained cell pellet was washed twice with cold PBS and centrifuged at 1200 rpm, followed by resuspending the obtained cell pellet into 600 μL of annex buffer (1×) that contained a combination of Alexa Fluor 488 – Annexin V (5 μL) and propidium iodide (1 μL) prepared from stock of 100 μg ml^{-1}. The combination was incubated for 15 min at room temperature protected from light before the cells were analysed using flowcytometry.

3.5. *In vivo* investigation

All animal procedures were performed in accordance with the Guidelines for Care and Use of Laboratory Animals by the UK Animals (Scientific Procedures) Act, 1986 and approved by the Animal Ethics Committee of Ulster University.

B16 melanoma cells were grown in large amounts (~5 million cells per 75 ml flask) for implanting subcu-

taneously into the rear dorsum of the mice. Once the cells reached a confluency of 75–80%, ensuring they were in a continuously growing state, they were harvested by trypsinization using 10% trypsin in sterile filtered PBS. Upon counting the cells, the obtained cell pellet was resuspended in sterile filtered PBS so that 3×10^6 B16 cells per ml were obtained. A 100 μl aliquot of this cell suspension was injected subcutaneously into the rear dorsum of the CD-1 nude mice. Mice were assessed daily for tumour burden, weight and general health throughout the period of the study.

3.5.1. *In vivo* PDT investigation. The CD-1 nude mice used in the study were 50% males and 50% females. They had an average weight of 27.6 ± 6.5 g and were 10–12 weeks old. After implanting the mice with B16 cells they were monitored on a daily basis with the study commencing when the tumours were visible, measurable and had reached an average volume of 41.97 ± 2.68 mm^3. The tumours reached this size in 3–4 days after implantation.

The preparation of the required formulation for injection and the murine model was done simultaneously and prior to starting the PDT treatment *in vivo*. The animals were divided into 3 groups with 5 animals selected for each group, selection was based on tumour size, to ensure that the average tumour size remained the same throughout the groups and that the range included within each group was similar, additionally, no group had less than two from any particular gender. These groups were – untreated, the animals which did not receive any dosing; RB-K2, where the animals received the unencapsulated form of RB-K2 and PS-RB-K2, where the animals received the PS encapsulating RB-K2 at an identical concentration to the unencapsulated drug, in addition to receiving the photosensitiser peptide conjugate, these groups also received light treatment to activate the photosensitiser (1 mM solution of RB-K2 in PBS). The treatment was carried out on day 0, 3, and 7. The samples, for the required groups, were administered directly into the tumour with the volume of drug solution administered ranging between 20 μl and 75 μl. The required volume was calculated based on half of the tumour volume calculated to a nearest 10. After the drug was administered, it was followed by an immediate dose of light treatment (Fenix LD01, LED, 3 min, 68.4 J cm^{-2}) without any delay, followed by a second dose of light (Fenix LD01, LED, 3 min, 68.4 J cm^{-2}) after 1 hour.

3.5.2. Real time *in vivo* imaging (IVIS) of RB-K2 and PS-RB-K2 following intra-tumoral injection. *In vivo* imaging was achieved by injecting 100 μL (1 mM) of RB-K2 and 50 μL (1 mM) of PS-RB-K2 directly into the tumours with the injection volume calculated depending on the tumour size, (half of the calculated tumour volume to a nearest 10, with a maximum injection volume of 100 μL). The animal was then placed into Xenogen IVIS® lumina imaging system chamber which maintained at 37 °C. The imaging filters were set to excitation wavelength of 535 nm and emission wavelength of 580 nm, a wavelength close to the excitation of rose bengal. The fluorescence of injected samples was monitored every hour for 4 h and then every 24 h till the samples were depleted. The images were then analysed using Living Image software version 2.60.

3.5.3. Analysis of quenching effect of RB-K2 with and without encapsulation. The study was conducted by preparing different concentrations of RB-K2 and PS-RB-K2 in PBS, ranging from 0.005 μM to 1 mM and recording both the absorbance (at 570 nm) and the corresponding fluorescence emission at 590 nm using Fluostar Omega microplate reader. Sample concentrations and subsequent absorbance and fluorescence data were then used to plot the graphs.

3.6. Statical analysis

All the statical analysis were done using GraphPad Prism 5 (v5.01), and Microsoft Excel for Microsoft 365 MSO (Version 2507). Statical differences were analysed using one-tailed student *t*-test, with * denoting p value < 0.05, ** $p < 0.01$, ***$p < 0.001$ and highest significance denoted as **** with p value < 0.0001, a non-significant difference was shown as ns.

4.0. Results and discussion

4.1. Synthesis and characterisation of RB-K2

RB-K2, Fig. 1a, was synthesised by solid phase peptide synthesis, using a rink amide resin. Amino acids were subsequently added to the linker in a chain like fashion through the creation of new amide bond formations, before an octanoic acid derivative of RB was added and the compound cleaved from the resin following the deprotecting of any side chain protecting groups (Boc, Trt) by trifluoracetic acid (TFA). The resulting pink solid was purified using prep hplc (Fig. 1b) and the compound confirmed using MALDI TOF MS, with the anticipated mass of 2724 Da (Fig. 1c).

4.2. Formulation and characterisation of PS-RB-K2

The polymer was synthesised according to the method described in the previous publication by Martin *et al.* (2016),[26] with the schematic representation depicted in Fig. 2a. The polymer was prepared from a hydrophobic and hydrophilic monomer, the hydrophobic decyl methacrylate (compound **3**, Fig. 2a) was synthesised from decanol *via* an esterification reaction with methacrylic acid whereas the hydrophilic PEG methacrylate (M_n 500) (compound **4**, Fig. 2a) was purchased and used without further modification. The prepared polymer was of random configuration so the alignment of each monomer within the polymeric structure may vary. Parameters affecting the final polymer, such as the amount of each monomer used, temperature, time and amount of initiator used for the reaction were kept consistent resulting in a controlled reaction with reproducible results. Importantly, the molar ratio between the hydrophobic and hydrophilic moieties remained consistent at 3 : 5[27] with 37.5% w/w hydrophobic decyl monomer and 62.5% w/w hydrophilic PEG methacrylate, resulting in an amphiphilic random copolymer as depicted in compound **5**, Fig. 2a.

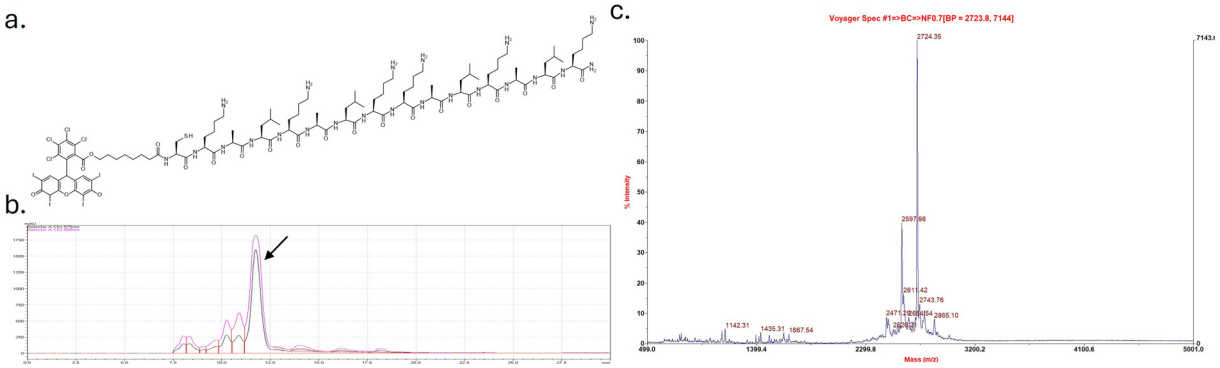

Fig. 1 (a) Chemical structure of RB-K2, rose bengal conjugated *via* an 8-carbon spacer to the amphiphilic peptide C(KALKALK)2. (b) Preparative HPLC trace of RB-K2, the pure compound peak detected between 11.0–12.5 minutes observed at 560–575 nm. (c) MALDI-TOF-MS spectra of pure peptide conjugate RB-K2 showing obtained mass of 2724.35 Da (calculated for $C_{103}H_{161}Cl_4I_4N_{22}O_{21}S$ = 2725.01 g mol^{-1}). Acquired on Voyager instrument in positive ion mode using CHCA matrix.

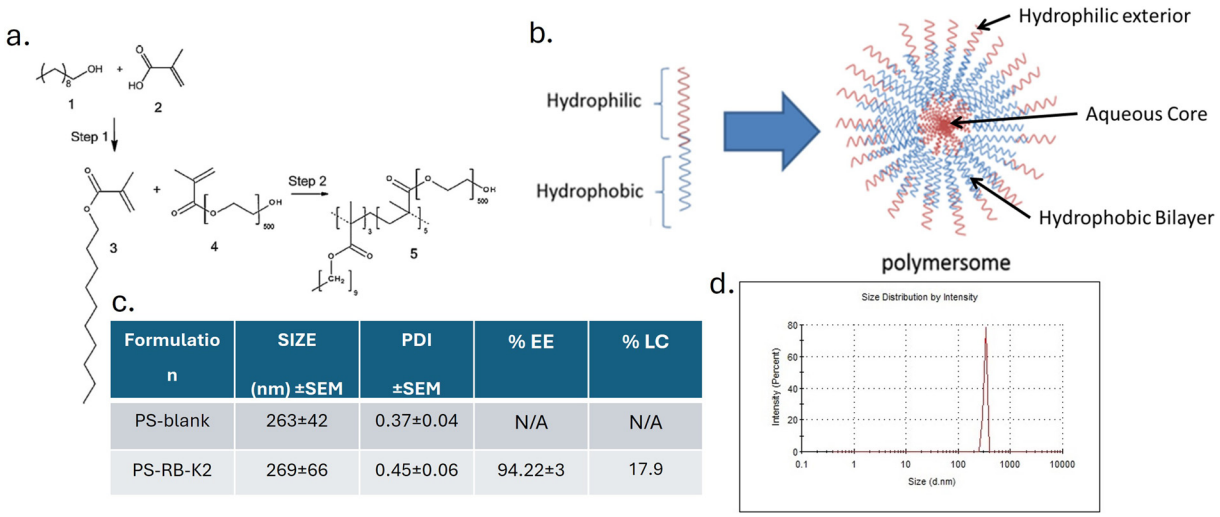

c.

Formulation	SIZE (nm) ±SEM	PDI ±SEM	% EE	% LC
PS-blank	263±42	0.37±0.04	N/A	N/A
PS-RB-K2	269±66	0.45±0.06	94.22±3	17.9

Fig. 2 (a) Schematic representation of the production of the decyl (hydrophobic monomer) **3** from the creation of decanol (1) and methacrylic acid (2) in step 1 and the subsequent polymerisation in step 2 resulting from the addition of the decyl monomer (3) and PEG methacrylate (M_n 500 (4)). (b) Illustration of polymersome creation from amphiphilic polymer, blue depicting the hydrophobic decyl moiety and red the PEG moiety. (c) Characterisation of polymersomes containing RB-K2 (PS-RB-K2) and compared with blank polymersomes (PS-blank) in terms of hydrodynamic radius (size) and polydispersibility index (PDI), encapsulation efficiency (EE) and loading capacity (LC) (n = 3). (d) Size distribution graph of PS-RB-K2.

There are several available methods, including the use of a microfluidic instrument, by which to prepare nanoparticles of this type with the hydrophilic corona and hydrophobic bilayer, illustrated in Fig. 2b. We have previously demonstrated that the reverse phase evaporation method (RPE) results in good size consistency, high stability, high drug encapsulation and a suitable PDI.[1] This method resulted in polymersomal nanoparticles with a similar hydrodynamic radius and PDI for both RB-K2 containing delivery systems, PS-RB-K2 and blank particles (PS-blank), Fig. 2c, and is comparable with polymersomes prepared with other compounds encapsulated.[1,25] The loading capacity is based on the encapsulation of 400 μM of RBK2 (1.09 mg ml^{-1}) encapsulated with 5 mg ml^{-1} polymer. The size distribution graph of PS-RB-K2 is presented in Fig. 2d.

4.3. *In vitro* analysis

The ability of RB-K2 to effectively destroy melanoma cells, using photodynamic therapy was first established *in vitro* using the B-16 melanoma cell line, Fig. 3a. The peptide conjugate by itself, at the highest concentration used in this study (5.0 μM) in the absence of light stimuli was found to be non-toxic to cells. At the lowest concentration of 0.1 μM, cell viability was found to be 91.8 ± 2.8% & 37.5 ± 6.7% when activated with 1- & 2 min light treatment respectively (22.8 and 45.6 J cm^{-2} total light dose respectively), indicating that using an increased light dose at lower concentration, *i.e.* 0.1 μM, could increase cellular toxicity by almost 50% (Dark-Ctrl *vs.* 0.1 μM RB-K2 + light 2 min, $p < 0.0001$,****), whereas at the higher concentrations of 1.0 & 5.0 μM almost 100% cell death ($p <$

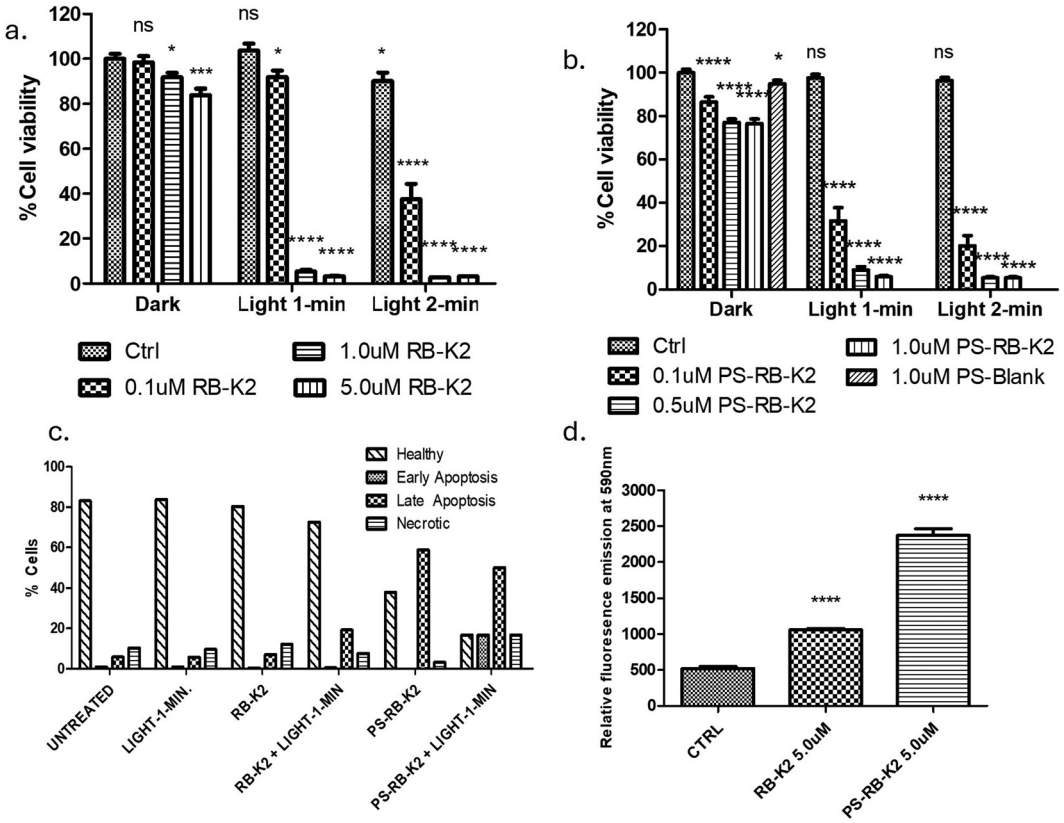

Fig. 3 PDT experiment showing % cell viability in B16 cells with varying concentrations of (a) RB-K2 and (b) PS-RB-K2, with and without administration of white light relative to cells containing no RB-K2 or PS-RB-K2. Without light administration shown as DARK and with light shown under light 1 min and Light 2 min, all compared against Dark-Ctrl which contains cells that received no treatment, (c) *in vitro* apoptosis assay in B16 cells using – 1 μM samples of each RB-K2 and PS-RB-K2. The experiment was carried out using samples in combination with or without 1 min light as a stimulus. The control groups were cells that received no treatment, or cells receiving only 1 min light. All were compared against healthy cells in individual groups. Each group was further categorised under health cells and dead cells (early apoptosis, late apoptosis, and necrosis). (d) An *in vitro* experiment showing cellular uptake of RB-K2 and PS-RB-K2 at 5 μM in B16 cells fluorescence emission recorded at 590 nm, with CTRL representing cells that received no treatment. For statistical analysis, groups were compared against cells that received no treatment *i.e.*, Dark-Ctrl in Fig. 1a, 1b and Ctrl in Fig. 1d. Error bars representing ± SEM (n = 12).

0.0001,****), was observed in both light activation conditions. Additionally, the cells are unaffected with light only treatment, as seen in the control cells containing no RB-K2 (Fig. 3a) or PS-RB-K2 (Fig. 3b) and irradiated with light (either 1 or 2 min) confirming that light is indeed an appropriate stimulus for allowing selectivity of effect. This result is in keeping with that previously reported.[24] The same experimental conditions were carried out for the polymersomal encapsulated RB-K2, PS-RB-K2. No observational differences were seen at the higher concentrations, as maximum cell death had already been established using the naked drug. The results at the lower concentration and those of the dark toxicity are of more interest, Fig. 3b. Dose dependent dark toxicity was observed in the control samples, this is most likely due to internalisation of K2, the peptide part of drug with the help of the PS through endocytosis. Research by Standley *et al.*, suggests a similar phenomenon where K2 was able to gain entry in breast cancer cells and cause cell death through incorporation of the peptide into nanofibers, whereas the peptide K2 was unable to do so on its own.[28] At the lowest concentration of 0.1 μM RB-K2 encapsulated within the PS, PS-RB-K2, cell viability was found to be 31.6 ± 6.0% with 1 min light activation (Dark-Ctrl *vs.* 0.1 μM PS-RB-K2 + light 1 min, $p < 0.001$,***), compared to less than 60% for free drug. Not surprising, at the higher dose of light a higher cell death was reported. A similar study was completed in B-16 melanoma cells using only RB, without the peptide, as well as polymersomal RB (PS-RB) and polymersomes containing both RB and the K2 peptide, but not conjugated together, known as PS-RB + K2. The results of these studies are given in the SI data (S1–S3). It can be concluded from these studies that the RB-K2 conjugate is a requirement for enhanced PDT to occur, with the encapsulation with a polymersome, significantly enhancing its efficiency.

The production of reactive oxygen species (ROS) caused by Type II photochemical reactions within PDT is well documented.[29] To confirm the production of ROS, the singlet oxygen scavenger, singlet oxygen sensor green (SOSG) was incubated with cells following exposure with either no drug, RB-K2 or PS-RB-K2. All samples were activated with white light before the fluorescent emission of SOSG was assessed.

Unsurprisingly, both RB-K2 and PS-RB-K2 cells had an increased fluorescence emission relative to no drug compound present, with PS-RB-K2 showing a 27.6% increase in relative emission compared with 19.5% of the unencapsulated RB-K2 (SI data, S4). The resultant oxidative damage means that PDT can trigger both modes of cell death, apoptosis and necrosis in target cells. Apoptosis is an active, controlled and energy-requiring process and therefore contrasts necrosis, which is an entropic event and in most cases a consequence of loss of membrane integrity and metabolic homeostasis.[29] An apoptosis assay was carried out with and without light activation of both RB-K2 and PS-RB-K2 in B16 cells to detect and quantify biological processes involved with programmed cell death. Apoptosis assay uses dye combination (Annexin V and propidium iodide) which segregate healthy cells from dead cells (in form of early apoptosis, late apoptosis, and necrosis).[30] The graph obtained can be seen from Fig. 3c. As expected, most of the cells remain healthy in the untreated group (received no treatment), the group treated with light-1 min (received only light), and the group receiving RB-K2 (received 1 μM of RB-K2 without activation with light). The unactivated encapsulated RB-K2 group showed healthy cells reduced to 72.63% and an increase in late apoptosis accounting for 19.22%, confirming what was observed in the cell viability assay in Fig. 3b, and likely due to the enhanced uptake of the mitochondrial disrupting peptide that forms part of the RB-K2 compound. As expected, both the light activated compounds showed the highest amount of apoptosis with the encapsulated PS-RB-K2 formulation treated with light proven to be the most affected, with only 16.67% cells remaining healthy while 50% cells were seen to affected by late apoptosis, 16.67% were in the process of early apoptosis and 16.67% cells necrotic.

In order to confirm that the increase in cellular toxicity is indeed a direct result of enhanced cellular uptake of the nanoparticle, B-16 cells were incubated with 5 μM of either RB-K2 and PS-RB-K2 for 3 h after which the cells were washed twice with PBS and the fluorescence emission was noted at 590 nm. The results obtained can be seen from Fig. 3d, which shows an accumulation of PS-RB-K2 almost 2.5 times more than RB-K2 at the same concentration and incubation duration suggesting the encapsulation of RB-K2 within Ps helps with enhancing the uptake and hence increase cell death produced by PDT.

Based on these positive *in vitro* results, the next step was to investigate if this effect was translated *in vivo*. However, prior to this study, we were keen to establish the optimal light activation conditions. In our previous experiments we had repeatedly observed that two minutes of light activation were superior to one minute. To further understand the excitation process, we exposed B-16 cells containing either RB-K2 or PS-RB-K2 to 2 min continuous light treatment or 2 min light treatment delivered as two 1 min treatments with a break in between. The results obtained, displayed in Fig. 4, would suggest that the light activation regime is of significant importance when optimising efficacy. The encapsulated drug shows an increase in cell death by 26.2% in cells containing PS-RB-K2, when subjected to two subsequent treatments of 1 min light (each given at a difference of 30 min (1 + 1 min light)) when compared with excitation by a continuous 2 min light treatment (2 min light). The cell viability reduced to 35.09 ± 2.1% (1 + 1 min light) (****$p < 0.0001$) and 61.3 ± 5.0% (2 min light) (**$p < 0.01$). A similar trend was seen in the cells treated with unencapsulated or free drug (RB-K2) which displayed a difference of 39% in cell viability, with the cell viability determined to be 24.6 ± 6.2% (****$p < 0.0001$) with exposure to 1 + 1 min LED compared with 63.6 ± 12.1% (*$p <$

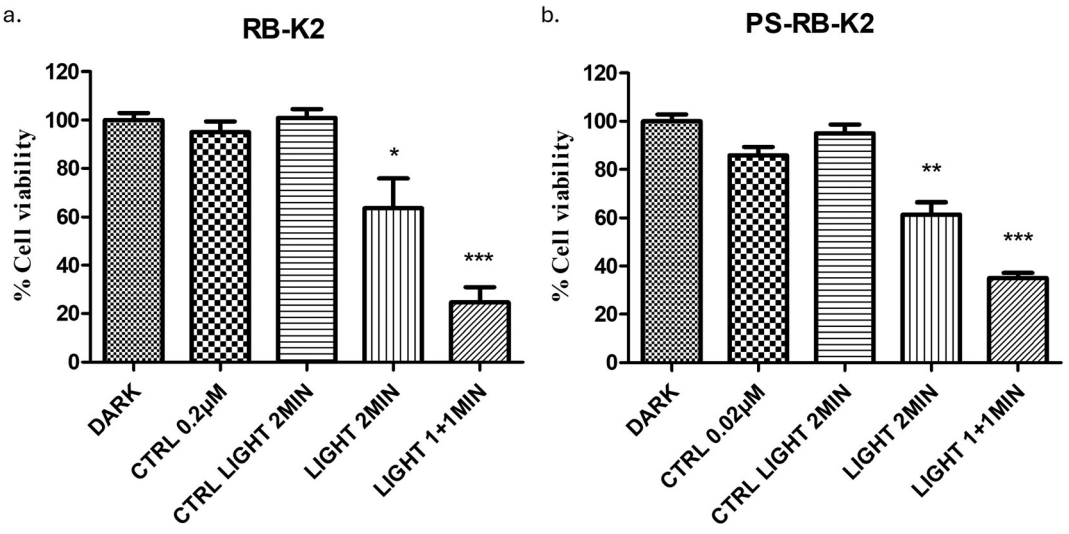

Fig. 4 PDT experiment showing % cell viability in B16 cells (a) shows similar experiment carried out using free drug of RB-K2 at 0.2 μM, there was a high significant difference observed between dark *versus* 0.2 μM light 1 + 1 min. (b) shows treatment with 0.02 μM of P-RB-K2 with conjugation of light for (2 min and 1 + 1 min) and without conjugation of light (Ctrl 0.02 μM) as external stimuli, (Ctrl light 2 min) used as control for the response generated by light dose only, all relative to cells (dark) that contain no PS-RB-K2 and without light conjugation. Error bars represent ± SEM ($n = 12$).

0.05) cell death when exposed to 2 min light. This study confirms that when the light dose is given at two separate intervals this is superior to giving one single outright dose of light. This is perhaps unsurprising as the availability of oxygen present in the surroundings of the cells during light treatment directly impacts the quantum yield of reactive oxygen species produced and in turn impacts the photodamage caused by the photosensitiser.[31]

4.4. *In vivo* analysis

After establishing the benefit of two subsequent doses of light for the activation of PDT in the treatment of melanoma cells *in vitro*. This knowledge was used to design an *in vivo* experiment to further support the information, where activation of the photosensitiser would be achieved using two light doses of 3 min delivered with a 1-hour interval was given after administering the samples of either PS-RB-K2 or RB-K2. In addition to the change in light activation, the treatments would be administered through intralesional injection directly into the tumours. Our previous studies had confirmed that although a significant amount of PEG based polymersomes accumulates in the tumour microenvironment, they were mainly eliminated from the liver and to a lesser extent the kidneys.[25] Intralesional injections ensure that 100% of the drug reaches the site of administration, and is common practice for melanoma cancer treatment, such as with the administration of T-VEC (Talimogene laherparepvec) a genetically modified virus that activates T-cells and enhance the effect of immunotherapies.[32] Additionally, photosensitivity is minimised to a smaller area through local administration. As the change was made from intravitreal to intralesional, then it was imperative that the volume of drug administered was calculated based on the volume of the tumour at the time of administration (this is common practice for T-VEC administration). After the drug was administered, it was followed by an immediate dose of light treatment (3 min) without any delay, followed by a second dose of light (3 min) after 1 hour. The treatment was carried out on days – 0, 3, and 7 (total light dose at each activation 68 J cm^{-2}).

The change in tumour volume was recorded over a period of 10 days. The obtained results could be seen from the graph in Fig. 5(a), with the control group of untreated tumours being the same control used in accordance with the 3Rs. The melanoma cancer cell line, is a particularly aggressive form of cancer, as evidenced by a doubling rate of anywhere between 14–24 hours.[33] The control group shows as average increase in tumour volume of 2498 ± 792%. Averaged over the 10 days of the experiment, this equates to an increase of 114% each day, which is a doubling time of 21 h, and expected from an aggressive cancer cell line such as B16. A tumour volume increase of 443 ± 113% was observed in the group treated with the unencapsulated or free drug, equating to an average tumour volume increase of 14% in 24 h, reducing the doubling time from 21 h to 166 h, ~7 days. This is a vast reduction in tumour growth rate for an aggressively growing cell line. Most impressively, was the tumour control of the mice in the treatment group treated with PS-RB-K2. The average tumour growth at the end of the experiment was 42 ± 22%, with two of the five mice seeing a significant reduction in tumour volume. The average daily change in tumour volume was −2%, meaning that a doubling rate cannot be calculated for this treatment regime and suggesting an effective treatment option for melanoma cancer using PDT. The tumours were excised at the end of the experiment, Fig. 5b, the tumour growth control is evident from those tumours treated with RB-K2 and light, with the reduction in volume for those treated with PS-RB-K2 and light resulting in an increase in the effectiveness of PDT for melanoma with the additional benefit of a nanoparticle drug delivery system.

The weight change was also recorded over the period which can be seen from Fig. 5c. The graph suggests a very minor to almost no weight change over the 10 days period of the study. Animals in untreated group maintained the weight of 98 ± 2%

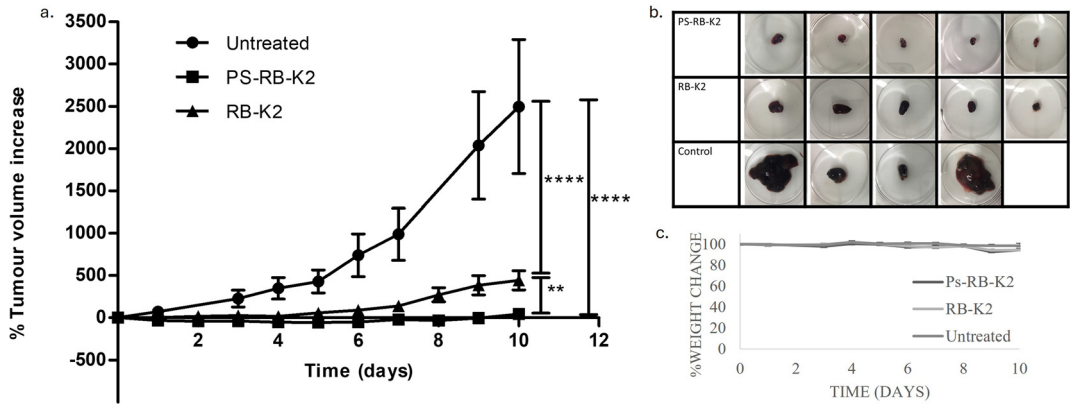

Fig. 5 CD-1 nude mice bearing B16 tumours treated with 1.0 mM RB-K2 with and without polymersomal encapsulation (5 mg ml^{-1} polymer), volume injected was calculated based on half of the tumour volume calculated to a nearest 10, with a maximum of 100 microlitres delivered. 3 min white led light was shown on the tumour immediately and again following 1 h. The treatment was done on day – 0, 3 and 7. (a) Tumour growth presented as % vol. increase over 10 days. (b) Photograph of excised tumours. (c) Growth chart for each condition, showing no significant weight loss. Error bars represent ± SEM (n = 4 untreated and n = 5 treatment groups).

on day 10 compared to day 0 of the treatment. The animals treated with RB-K2 had a weight of 94 ± 1% and animals administered PS-RB-K2 weighed 94 ± 1% on day 10 compared to initial weight on day 0.

The combination of *in vitro* and *in vivo* experiments, allow us to conclude the enhanced efficiency of RK-K2 with the use of a nanosized polymersomal drug delivery system, PS-RB-K2. The increased cellular uptake undoubtedly has a positive impact on this increased efficiency, however there may be other mechanisms involved, for example, nanoparticles are well known to exert a protective effect on their cargo as well as benefitting from the EPR (enhanced permeation and retention) effect within tumour tissue. To confirm the EPR effect with PS-RB-K2 we were able to observe in real time the fluorescence emission of both RB-K2 and PS-RB-K2 in the mice with the help of IVIS (*In Vivo* Imaging Systems) study using the fluorescence of RB. The results obtained from the IVIS study (Fig. 6a, quantified in Fig. 6b) show an obvious increased fluorescence emission of RB in tumours treated with the encapsulated PS-RB-K2 when compared with the free drug. It should be noted that the fluorescence emission is from the RB moiety of RB-K2 only, and therefore it is not possible to ascertain whether the compound is still intact. On initially inspection, it would appear that the EPR effect is clear from the IVIS images presented. However, it is well documented that photosensitisers are retained preferentially within the tumour microenvironment, and therefore one might not expect to see such a significant variation, especially given that the route of delivery was directly into the tumour itself.

The cause of this variation in RB fluorescence was further studied by analysing the absorbance and emission spectrum of both samples of RB-K2 and PS-RB-K2 at varying concentrations. From the obtained results we can see that as the concentration of both formulations is increased, so too does the absorbance (Fig. 6c). This is as expected due the Beer Lambert Law where absorbance is directly proportional to the concentration. Interestingly, given the logarithmic scale (to allow direct comparison of a larger concentration range), the shape of the unencapsulated graph would appear to contain a linear region at higher concentrations whereas the encapsulated compound appears more as an exponential curve. However, the most interesting results are obtained from the emission data, Fig. 6d. When we increase the concentration of the unencapsulated compound, RB-K2, there is minimal increase in the emission recorded, this is not the case when we compare it with the fluorescence emission of the encapsulated compound, PS-RB-K2, at the same concentration range. One possible explanation for this is that self-quenching is occurring within the unencapsulated solution. A similar observation was reported by Chang *et al.* who attributed the lack of fluorescence emission to aggregation of RB which occurred at concentrations greater than 50 μM, due to the π–π stacking

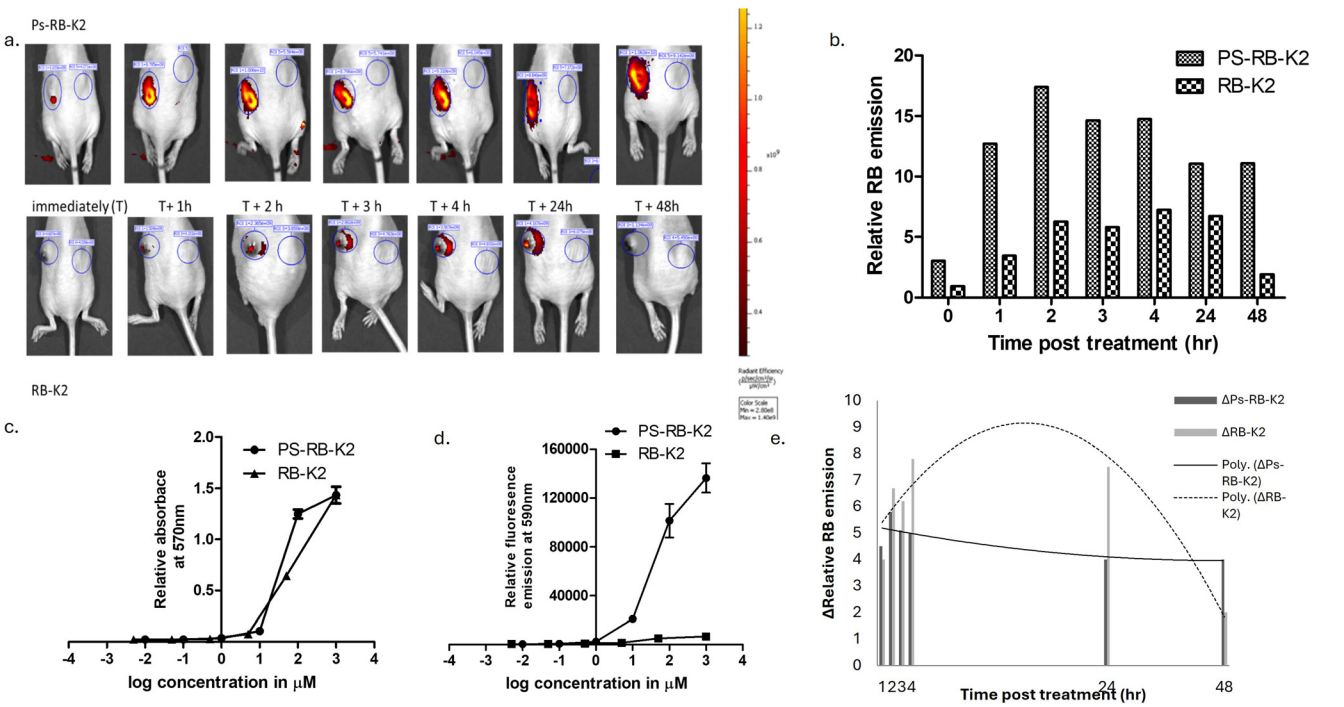

Fig. 6 (a) *In vivo* imaging of RB fluorescence mice bearing B-16 tumours treated *via* intratumoral injection of either RB-K2 or PS-RB-K2. Images were recorded at various time intervals indicative of the accumulation of the samples within in tumour tissue of the mice with the intensity scale given on the right of image. (b) Relative emission of RB from ivis images, relative to control area shown on dorsal images comparing post RB and PS-RB-K2 treatment. (c) Absorbance spectra of RB-K2 and PS-RB-K2 at 570 nm against concentration. Error bars representing ± SEM (n = 6) (d) fluorescence emission of RB-K2 and PS-RB-K2 at 590 nm against concentration error bars representing ± SEM (n = 6). (e) Change in relative emission over time of RB from IVIS images relative to control area shown with trend lines.

between the benzene ring structure of the RB.[34] A further study by Tomasini *et al.*, suggests that the fluorescence quantum yield of RB in water (0.018), could be increased to 0.13 by embedding RB on the surface of microcrystalline cellulose beads which implies that increasing the distance between the molecules could impact the overall fluorescence produced.[35] Therefore, due to the effect of the encapsulation on the fluorescence of the RB, it is more appropriate to measure the change in relative fluorescence emission over time, the results of which are displayed in Fig. 6e. From these results we can conclude that the PS-RB-K2 delivery system does indeed provide a prolonged retention, thus rendering it potentially suitable for daylight PDT. In addition, the sustained nature of the RB-K2 encapsulated within the polymersome is indicative of protection offered to the compound from enzymatic degradation. Therefore, we would conclude that the increased efficacy is most likely due to a combination of increased cellular uptake, retention within the tumour environment and protection from degradation.

5.0. Conclusion

This study successfully demonstrates that encapsulating the peptide-photosensitiser RB-K2 within a polymersomal nanocarrier significantly enhances the efficacy of photodynamic therapy for melanoma. The encapsulated formulation, PS-RB-K2, exhibited superior cellular uptake, light-induced cytotoxicity, and tumour growth suppression compared to the free conjugate. Mechanistically, the enhanced efficacy is attributed to increased cellular internalization, protection from photobleaching and degradation, and improved tumour retention—confirmed *via* IVIS imaging and fluorescence analysis. Moreover, optimization of the light dosing strategy (split activation) further augmented therapeutic outcomes. Together, these findings highlight the potential of PS-RB-K2 as the third generation of PDT with the first white light activated peptide photosensitiser for melanoma, bringing the technology closer to clinical translation.

While this study provides compelling evidence that polymersomal encapsulation markedly enhances the therapeutic performance of RB-K2 for melanoma PDT, several limitations must be acknowledged. Firstly, the *in vitro* work was limited to a single murine melanoma cell line (B16), with *in vivo* validation restricted to a subcutaneous B16 tumour model in CD-1 nude mice. Although this model is well established for assessing local drug response, it does not fully replicate the biological heterogeneity or immunological complexity of human melanoma. Second, the therapeutic studies relied exclusively on intratumoural administration. This approach maximises local drug exposure and is clinically meaningful for accessible cutaneous lesions, but it does not address the challenges associated with systemic delivery, distribution, and clearance. Evaluation of intravenous or topical delivery routes will be important to determine whether PS-RB-K2 can effectively accumulate in deeper or metastatic lesions and whether the enhanced tumour retention observed here remains evident under physiological circulation. Thirdly, although we can attribute the improved efficacy of PS-RB-K2 to enhanced cellular uptake, protection from quenching, and prolonged tumour retention, detailed mechanistic confirmation remains necessary. The precise endocytic pathways responsible for nanoparticle internalisation, the intracellular fate of the polymersomes, and the subcellular localisation of RB-K2 were not directly characterised. This level of understanding will help to advance the commercialisation of the technology. Finally, the safety profile of PS-RB-K2 requires further exploration. Body weight remained stable across groups, suggesting minimal acute toxicity; however, comprehensive toxicological evaluation —including haematology, serum chemistry, organ histopathology, and long-term safety—is essential prior to translational development. Additional investigation into the scalability and manufacturability of the polymersomal system will also be important, particularly with regard to solvent use, batch consistency, and regulatory considerations for PEG-based nanocarriers.

Collectively, these next steps will help define the translational potential of PS-RB-K2 and support the advancement of this white-light-activated, polymersome-enhanced PDT platform towards clinical application in melanoma. The research presented herein lays important groundwork, but meaningful challenges remain to be addressed.

Conflicts of interest

There are no conflicts to declare.

Data availability

Data will be made available on request.

Supplementary information (SI) is available on the *in-vitro* cell viability studies of the individual components used within this study as well as a singlet oxygen sensor green (SOSG) study. See DOI: https://doi.org/10.1039/d5pm00259a.

Acknowledgements

The authors would like to acknowledge Innovation Ulster Limited (IUL) for financial assistance. This work was funded by Innovate UK (10129806, 10087520 and 10069041).

References

1 N. Aibani, T. N. Khan and B. Callan, Liposome mimicking polymersomes; A comparative study of the merits of polymersomes in terms of formulation and stability, *Int. J. Pharm.:X*, 2020, **2**, 100040.

2 J. F. Le Meins, O. Sandre and S. Lecommandoux, Recent trends in the tuning of polymersomes' membrane properties, *Eur. Phys. J. E.*, 2011, **34**(2), 14.
3 D. E. Discher and A. Eisenberg, Polymer vesicles, *Science*, 2002, **297**(5583), 967–973.
4 L. L. Osorno, A. N. Brandley, D. E. Maldonado, A. Yiantsos, R. J. Mosley and M. E. Byrne, Review of Contemporary Self-Assembled Systems for the Controlled Delivery of Therapeutics in Medicine, *Nanomaterials*, 2021, **11**(2), 278.
5 A. Saneja, A. K. Panda and E. Lichtfouse, ed., *Sustainable Agriculture Reviews 43: Pharmaceutical Technology for Natural Products Delivery Vol. 1 Fundamentals and Applications*, Springer Nature, 2020, pp. 161–215.
6 F. Meng, Z. Zhong and J. Feijen, Stimuli-responsive polymersomes for programmed drug delivery, *Biomacromolecules*, 2009, **10**(2), 197–209.
7 X. Hu, Y. Zhang, Z. Xie, X. Jing, A. Bellotti and Z. Gu, Stimuli-responsive polymersomes for biomedical applications, *Biomacromolecules*, 2017, **18**(3), 649–673.
8 Y. Wei, X. Weng, Y. Wang and W. Yang, Stimuli-Responsive Polymersomes: Reshaping the Immunosuppressive Tumor Microenvironment, *Biomacromolecules*, 2024, **25**(8), 4663–4676.
9 C. N. Krasner, S. M. Campos, C. L. Young, K. R. Chadda, H. Lee, M. J. Birrer, N. S. Horowitz, P. A. Konstantinopoulos, A. M. D'Ascanio, U. A. Matulonis and R. T. Penson, Sequential Phase II clinical trials evaluating CRLX101 as monotherapy and in combination with bevacizumab in recurrent ovarian cancer, *Gynecol. Oncol.*, 2021, **162**(3), 661–666.
10 T. Hamaguchi, A. Tsuji, K. Yamaguchi, K. Takeda, H. Uetake, T. Esaki, K. Amagai, D. Sakai, H. Baba, M. Kimura and Y. Matsumura, A phase II study of NK012, a polymeric micelle formulation of SN-38, in unresectable, metastatic or recurrent colorectal cancer patients, *Cancer Chemother. Pharmacol.*, 2018, **82**(6), 1021–1029.
11 I. Peciu-Florianu, Q. Vannod-Michel, E. Vauleon, M. E. Bonneterre and N. Reyns, Long term follow-up of patients with newly diagnosed glioblastoma treated by intraoperative photodynamic therapy: an update from the INDYGO trial (NCT03048240), *Neuro-Oncology*, 2024, **168**(3), 495.
12 M. Clinic, *EUS-guided verteporfin photodynamic therapy for locally advanced pancreatic adenocarcinoma*, 2023. https://ClinicalTrials.gov.
13 C. Compagnin, F. Moret, L. Celotti, G. Miotto, J. H. Woodhams, A. J. MacRobert, D. Scheglmann, S. Iratni and E. Reddi, Meta-tetra(hydroxyphenyl)chlorin-loaded liposomes sterically stabilised with poly(ethylene glycol) of different length and density: characterisation, in vitro cellular uptake and phototoxicity, *Photochem. Photobiol. Sci.*, 2011, **10**(11), 1751–1759.
14 R. W. Wu, C. M. Yow, E. Law, E. S. Chu and Z. Huang, Effect of Foslip® mediated photodynamic therapy on 5-fluorouracil resistant human colorectal cancer cells, *Photodiagn. Photodyn. Ther.*, 2020, **31**(101945), 5.
15 Z. Liu, Y. Zhong, X. Zhou, X. Huang, J. Zhou, D. Huang, Y. Li, Z. Wang, B. Dong, H. Qiao and W. Chen, Inherently nitric oxide containing polymersomes remotely regulated by NIR for improving multi-modal therapy on drug resistant cancer, *Biomaterials*, 2021, **277**, 121118.
16 C. Lim, J. K. Kang, W. R. Won, J. Y. Park, S. M. Han, T. N. Le, J. C. Kim, J. Her, Y. Shin and K. T. Oh, Co-delivery of D-(KLAKLAK) 2 peptide and chlorin e6 using a liposomal complex for synergistic cancer therapy, *Pharmaceutics*, 2019, **11**(6), 293.
17 Z. Tang, W. Luo, M. Xu, Y. Liu, Q. Yu and L. L Wang, A TME-responsive oxygen-self-supplying hybridized polymersome for synergistic triple-modal therapy and precision theranostics in hypoxic tumors, *J. Mater. Chem. B*, 2025, **13**, 8136.
18 G. Cheng, S. Tao, S. Liu, P. Wang, C. Zhang, J. Liu, C. Hao, S. Wang, D. Guo and B. Xu, Glutathione-responsive polymersome with continuous glutathione depletion for enhanced photodynamic therapy and hypoxia-activated chemotherapy, *ACS Macro Lett.*, 2024, **13**(5), 599–606.
19 W. Yang, G. Zhu, S. Wang, G. Yu, Z. Yang, L. Lin, Z. Zhou, Y. Liu, Y. Dai, F. Zhang and Z. Shen, In situ dendritic cell vaccine for effective cancer immunotherapy, *ACS Nano*, 2019, **13**(3), 3083–3094.
20 Z. Lu, W. Jia, R. Deng, Y. Zhou, X. Li, T. Yu, M. Zhen and C. Wang, Light-assisted gadofullerene nanoparticles disrupt tumor vasculatures for potent melanoma treatment, *J. Mater. Chem. B*, 2020, **8**(12), 2508–2518.
21 Q. Tang, P. Hu, H. Peng, N. Zhang, Q. Zheng and Y. He, Near-infrared laser-triggered, self-immolative smart polymersomes for in vivo cancer therapy, *Int. J. Nanomed.*, 2020, 137–149.
22 M. Wang, B. M. Geilich, M. Keidar and T. J. Webster, Killing malignant melanoma cells with protoporphyrin IX-loaded polymersome-mediated photodynamic therapy and cold atmospheric plasma, *Int. J. Nanomed.*, 2017, 4117–4127.
23 M. C. Tsai, L. Y. Hsiao, Y. H. Chang, Y. H. Chen, S. H. Hu, C. Y. Hung and W. H. Chiang, Enhanced Intracellular IR780 Delivery by Acidity-Triggered PEG-Detachable Hybrid Nanoparticles to Augment Photodynamic and Photothermal Combination Therapy for Melanoma Treatment, *ACS Appl. Bio Mater.*, 2025, **8**(5), 3995–4007.
24 S. K. Dhillon, S. L. Porter, N. Rizk, Y. Sheng, T. McKaig, K. Burnett, B. White, H. Nesbitt, R. N. Matin, A. P. McHale, B. Callan and J .F. Callan, Rose bengal–amphiphilic peptide conjugate for enhanced photodynamic therapy of malignant melanoma, *J. Med. Chem.*, 2020, **63**(3), 1328–1336.
25 N. Aibani, H. Nesbitt, N. Marino, J. Jurek, C. O'Neill, C. Martin, I. Di Bari, Y. Sheng, K. Logan, S. Hawthorne, A. P. McHale, J. F. Callan and B. Callan, Electroneutral polymersomes for combined cancer chemotherapy., *Acta Biomater.*, 2018, **80**, 327–340.
26 C. Martin, N. Aibani, J. F. Callan and B. Callan, Recent advances in amphiphilic polymers for simultaneous deliv-

ery of hydrophobic and hydrophilic drugs, *Ther. Delivery*, 2016, **7**(1), 15–31.

27 I. Yildiz, S. Impellizzeri, E. Deniz, B. McCaughan, J. F. Callan and F. M. Raymo, Supramolecular strategies to construct biocompatible and photoswitchable fluorescent assemblies, *J. Am. Chem. Soc.*, 2011, **133**(4), 871–879.

28 S. M. Standley, D. J. Toft, H. Cheng, S. Soukasene, J. Chen, S. M. Raja, V. Band, H. Band, V. L. Cryns and S. I. Stupp, Induction of cancer cell death by self-assembling nanostructures incorporating a cytotoxic peptide, *Cancer Res.*, 2010, **70**(8), 3020–3026.

29 K. Plaetzer, T. Kiesslich, T. Verwanger and B. Krammer, The modes of cell death induced by PDT: an overview, *Med. Laser Appl.*, 2003, **18**(1), 7–19.

30 O. Kepp, L. Galluzzi, M. Lipinski, J. Yuan and G. Kroemer, Cell death assays for drug discovery, *Nat. Rev. Drug Discovery*, 2011, **10**(3), 221–237.

31 A. S. Vignion-Dewalle, N. Betrouni, J. B. Tylcz, M. Vermandel, L. Mortier and S. Mordon, Comparison of three light doses in the photodynamic treatment of actinic keratosis using mathematical modeling, *J. Biomed. Opt.*, 2015, **20**(5), 058001–058001.

32 P. F. Ferrucci, L. Pala, F. Conforti and E. Cocorocchio, Talimogene laherparepvec (T-VEC): an intralesional cancer immunotherapy for advanced melanoma, *Cancers*, 2021, **13**(6), 1383.

33 C. Danciu, A. Falamas, C. Dehelean, C. Soica, H. Radeke, L. Barbu-Tudoran, F. Bojin, S. C. Pînzaru and M. F. Munteanu, A characterization of four B16 murine melanoma cell sublines molecular fingerprint and proliferation behavior, *Cancer Cell Int.*, 2013, **13**(75), 1475–2867.

34 C. C. Chang, Y. T. Yang, J. C. Yang, H. D. Wu and T. Tsai, Absorption and emission spectral shifts of rose bengal associated with DMPC liposomes, *Dyes Pigm.*, 2008, **79**(2), 170–175.

35 E. P. Tomasini, S. E. Braslavsky and E. San Román, Triplet quantum yields in light-scattering powder samples measured by laser-induced optoacoustic spectroscopy (LIOAS), *Photochem. Photobiol. Sci.*, 2012, **11**(6), 1010–1017.